Ab Initio Insights on the Shapes of Platinum Nanocatalysts

Roman V. Chepulskii and Stefano Curtarolo*

Department of Mechanical Engineering and Materials Science, Duke University, Durham, North Carolina 27708, United States

ARTICLE

ABSTRACT Catalytic, chemical, optical, and electronic properties of nanocrystals are strongly influenced by their faceting. A variational approach based on quantum mechanical energies is introduced to evaluate stable and metastable shapes of Pt nanocrystals. The method leads to a nanoscale equation of state, which is solved self-consistently. It is found that the surface energy dependence on the lattice parameter is the key factor controlling the equilibrium stability of the crystal shapes. The variational approach, capable of predicting the changes in the hierarchy of crystals' shapes with respect to size, explains experimental results and establishes a new direction to search for better catalysts.

KEYWORDS: nanocatalysis · nanoparticles · first-principles · Wulff's construction · surface energy · surface tension

Catalysis plays a fundamental role in many fields of chemical and energy technologies.[1−6] The performance of catalysts is determined by their ability to control the rates and yields of chemical reactions (*i.e.*, to increase and reduce the amounts of desirable and undesirable products). Platinum and its compounds are among the most outstanding catalysts[1−7] as they have high density of electronic states at the Fermi level (essential for electron exchange for chemical reactions), and they are resistant to oxidation. Moreover, performance of Pt active nanoparticles can be tuned by modifying their shape.[8−10] Experimental observations for Pt nanoparticles usually report low-index facets,[7] although recently synthesized Pt tetrahexahedrons with high-index facets have been shown to have superior catalytic activity.[9] Despite attempts of *ab initio* analysis,[11,12] the observed variety of Pt nanoshapes has not been completely explained. The problem should be addressed because, in addition to interpreting experimental results, a rational explanation would help designing new shapes with superior chemical, optical, and electronic properties.[1−6,13] Furthermore, it would also contribute to understanding the general physics of the transition from bulk to nanoscale, important from both fundamental and technological points of view.[14−20]

The formidable task of predicting the shape of nanoparticles across a wide range of sizes can be partially tackled if we limit the interest to general knowledge of trends regarding shapes' phase transitions. With simple calculations of bulk and surface energies (values and variations), we can capture the energetic interplay between surface tension and elastic energy contributions. In this article, we present a rational first-principles approach describing the relative stability of different Pt nanoscale shapes. We consider the competition between elastic and surface energies for the seven shapes: the recently observed tetrahexahedron with (730) facets,[9] and the six most frequently observed shapes[7] that have (100) and (111) facets (cube, tetrahedron, octahedron, cuboctahedron, truncated octahedron, and truncated cube).

MODEL AND RESULTS

First, we calculate the relative quantum mechanical energies of six common Pt crystals shapes with up to 300−400 atoms. The relative crystal stability of the various shapes varies with size. This is shown in Figure 1a. Larger crystals with the six common shapes as well as the tetrahexahedron crystals are not addressed by *ab initio* means due to their high computational requirements.

To tackle larger crystals, we consider the energy of the finite system as a superposition of internal and surface energies (Figure 2). The energetic contribution of surface tension is described through the

*Address correspondence to stefano@duke.edu.

Received for review September 28, 2010 and accepted December 06, 2010.

Published online December 20, 2010.
10.1021/nn102570c

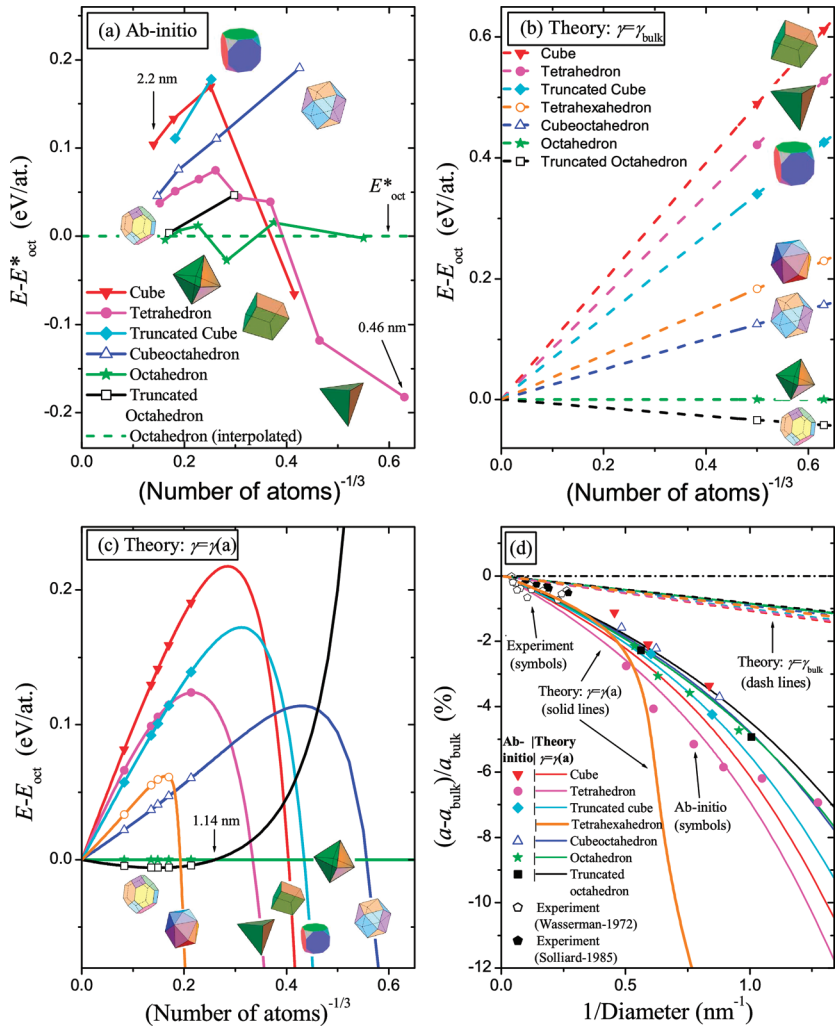

Figure 1. Size dependency of quantum mechanical energies and lattice parameters for the seven Pt crystals shapes. (a) *Ab initio*: ($E - E^*_{oct}$) where E^*_{oct} indicates the interpolation of the *ab initio* energies of the octahedron shapes. (b,c) *Variational*: ($E - E_{oct}$) with $\gamma = \gamma_{bulk} = \gamma(a_{bulk})$ and $\gamma = \gamma(a)$; E_{oct} indicates the corresponding variational value of the energy for the octahedron shapes; (d) $(a - a_{bulk})/a_{bulk}$ from experiments (symbols),[21,22] *ab initio* calculations (symbols), variational approach with $\gamma = \gamma_{bulk}$ (dashed lines) and $\gamma = \gamma(a)$ (solid lines). Relative energies and lattice parameters are presented with respect to corresponding values of octahedron nanoparticle and bulk, respectively.[23] The variational approach (a,c,d) is not applicable for sizes less than ~0.46 nm in diameter.

following self-consistent variational approach. The "nanoscale" equation of state (EOS) is defined as

$$E(a) = E_{bulk}(a) + \sum_{lmn} \gamma_{lmn}(a) S_{lmn}(a) \qquad (1)$$

where a is the lattice parameter, E_{bulk} is the energy of a bulk with the same number of atoms as in the crystal, γ_{lmn} and S_{lmn} are the surface energies and areas of the (lmn) facets. Within the variational framework, the equilibrium is determined by minimizing over the lattice parameter:

$$E = \min_a \{E(a)\} \qquad (2)$$

Thus, the energy and lattice parameter of the crystal are determined from the same nanoscale EOS, self-

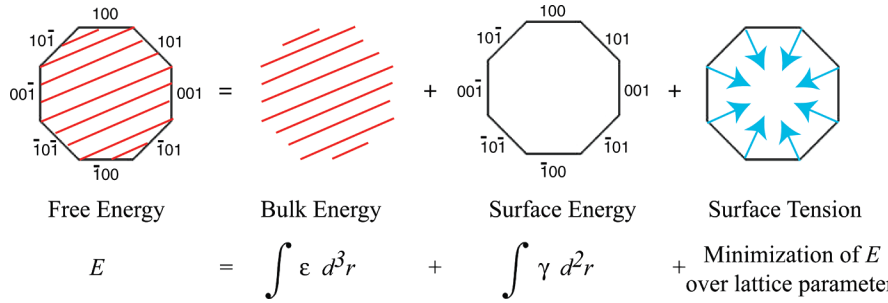

Figure 2. Proposed schematic decomposition of the finite crystal free energy E; ε is the density of bulk free energy, and γ is the surface energy. The variation of γ, surface tension, is balanced by the strain energy of the bulk.

consistently. It can be shown that for large crystals and parabolic "bulk" EOS, the solution of eq 2 is equivalent to the Stoneham[15] approach (see the Methods section). As we are interested only in trends, in this article, we neglect the high computationally demanding contributions to eq 2 such as substrate−particle interface energies, surrounding solvent interactions, and excess energies of edges and corners. Some of these contributions have predictable effects: overall, eq 2 tends to underestimate the particles' size. For instance, the excess energy of edges/corners would sum with $E(a)$ in eq 2, therefore leading to larger variational surfaces $S_{lmn}(a)$.

By fitting the bulk EOS[24] to the first-principles data (see the Methods section), $E_{bulk}(a)$ can be found. In order to determine the surface energies γ_{lmn} (lmn = 100,111,730), we calculate the quantum mechanical energies of the corresponding slabs for different lattice parameters (the slabs have enough layers to warrant convergence (see the Methods section)). According to eqs 1 and 2, the N layers, N atoms, slab energy $E^N_{slab(lmn)}$ for a given a can be expressed as

$$E^N_{slab(lmn)}(a) = NE^{at}_{bulk}(a) + \gamma_{lmn}(a)2S^{at}_{slab(lmn)}(a) \quad (3)$$

where $S^{at}_{slab(lmn)} = a^2K^{lmn}_{slab}$ is the (lmn) slab surface area per atom ($K^{100}_{slab} = 0.5$, $K^{111}_{slab} = 0.25\sqrt{3}$, $K^{730}_{slab} = 3.5(1 + (3/7)^2)^{1/2}$). Finally, the surface energies are obtained by inverting eq 3 leading to

$$\gamma'_{lmn}(a) \equiv \gamma_{lmn}(a)2K^{lmn}_{slab}a^2_{bulk} = (a_{bulk}/a)^2[E^N_{slab(lmn)}(a) - NE^{at}_{bulk}(a)] \quad (4)$$

Note that surface energies obtained from slabs are computationally more advantageous than if obtained from nanocrystals, although they do not contain energetic information about edges and corners. The dependencies of the self-consistent surface energies γ'_{lmn} (lmn = 100,111,730) with respect to the reduced lattice parameter, a/a_{bulk}, are depicted in Figure 3a. The corresponding *bulk* values of surface energies and surface tensions are in good agreement with values obtained previously by different methods (see the Methods section). Strikingly, the (100) and (730) bulk surface ener-

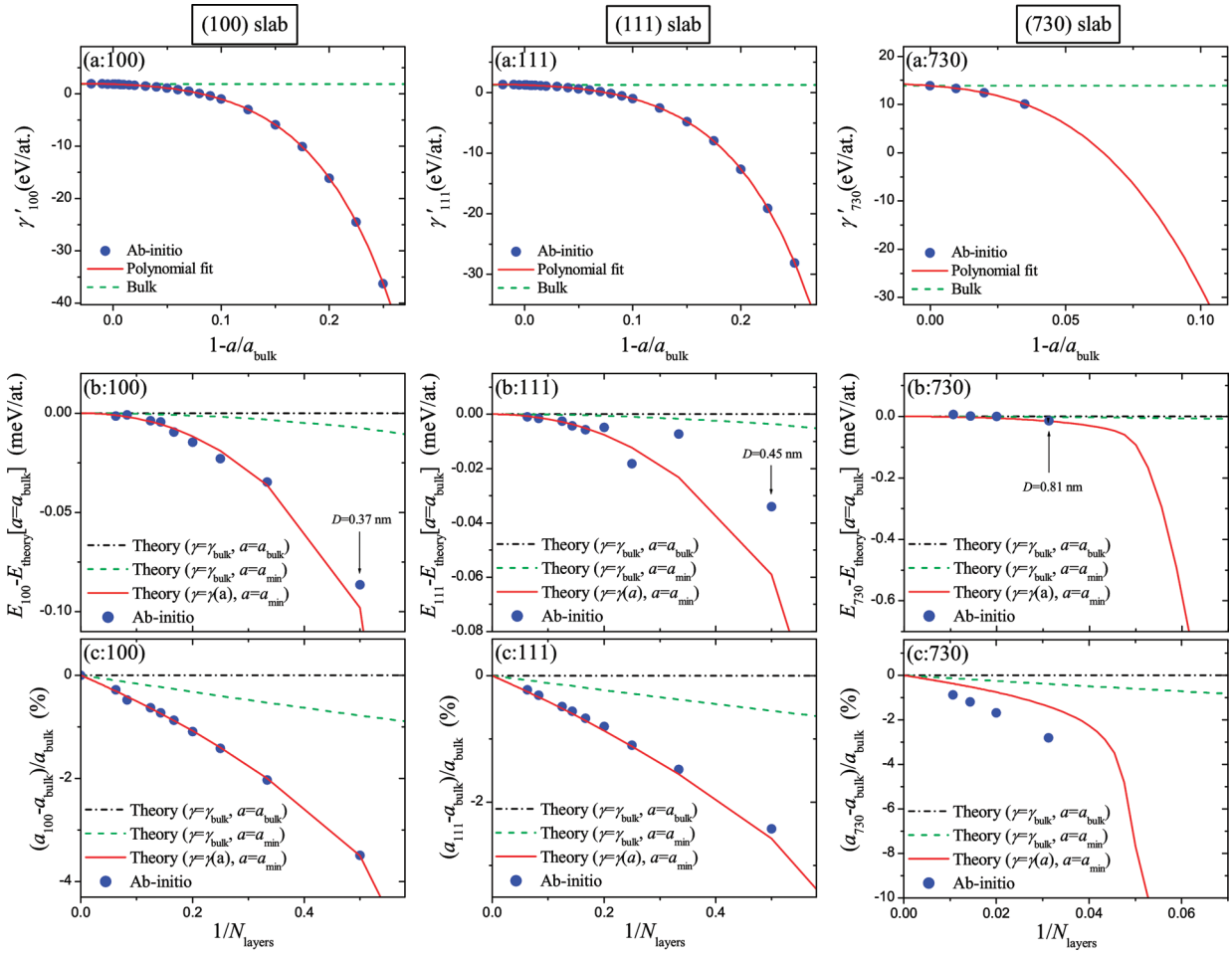

Figure 3. For (100), (111), and (730) slabs: (a) self-consistent surface energy γ'_{lmn} *versus* the reduced lattice parameter (a/a_{bulk}) as obtained from eq 4; (b) relative energies of the *relaxed* slabs *versus* the inverse number of slab layers from *ab initio* calculations and theoretical modeling with three different uses of eq 3: ($\gamma = \gamma_{bulk}$, $a = a_{bulk}$) indicates eq 3 without any minimization ($a = a_{bulk}$); ($\gamma = \gamma_{bulk}$, $a = a_{min}$) indicates eq 3 with minimization over a while keeping $\gamma = \gamma_{bulk}$; ($\gamma = \gamma(a)$, $a = a_{min}$) indicates eq 3 with complete minimization over a and with γ from eq 4; (c) relative lattice parameter of the *relaxed* slabs *versus* the inverse number of slab layers for the three cases of panels b.

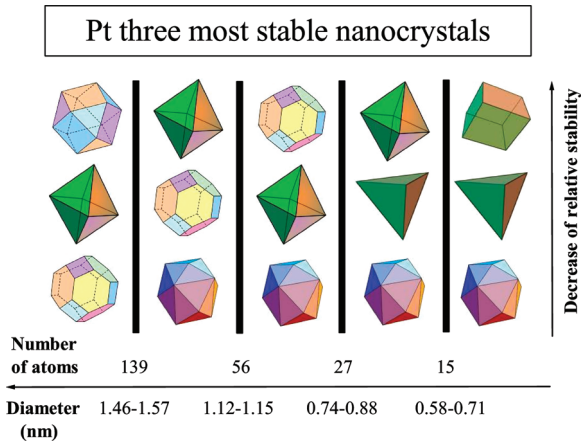

Figure 4. Three most stable crystal shapes of Pt as function of diameter. Shape transitions are predicted by the variational approach (Figure 1c). Note that the transitions based on *ab initio* results occur at slightly larger sizes (Figure 1a).

gies are found to be very similar. To verify the accuracy of the model for the description of the slabs, in Figure 3b,c, we show the relaxed slab energies and lattice parameters for different sizes. The largest differences are observed for very small slabs (2−3 layers for the (100) and (111) cases), which is explained by the fact that the surface energies were extracted from *ab initio* results obtained for larger slabs. Clearly, the theory gives adequate values for (100) and (111) slabs thicker than ~0.5 nm. In the (730) case, the values are less accurate as the calculations of large slabs are limited due to their high computational cost.

Figure 1c shows the relative crystal energies as functions of size calculated by substituting the values of eq 4 into eqs 1 and 2. Figure 1b depicts a similar scenario with the use of the bulk surface energies $\gamma_{bulk} = \gamma(a_{bulk})$. The lattice parameter as function of crystal size is presented in Figure 1d, and it is compared with *ab initio* and experimental values.

DISCUSSION AND CONCLUSIONS

The results of Figure 1 demonstrate that *the dependence of surface energies on the lattice parameter* provides sufficient qualitative agreement for the variational approach to *ab initio* results in a reasonably wide size interval. Moreover, the self-consistent lattice parameter values are also in good agreement with the *experimental* data available for large crystals (Figure 1d). The theoretical results for the tetrahexahedron shape can not be verified as the corresponding *ab initio* calculations would require the consideration of excessively large crystals. Two statements are relevant: (i) the use of bulk surface energies ($\gamma_{bulk} = \gamma(a_{bulk})$) is valid only for crystals with diameter larger than ~1.46−1.57 nm; (ii) the same limitation also applies when we use a linearized expression for lattice parameter through the bulk surface tension (shown in Methods section). Therefore, both approaches are not adequate to explain the changes in hierarchy of crystal energies *versus* sizes, as previously thought.

The limitation is overcome by using our variational approach to obtain the correct $\gamma(a)$. On the basis of the results of the *ab initio* calculations and the variational approach (Figure 1a,c), we address the most energetically stable Pt crystals for different sizes (Figure 4). For relatively large crystal (with more than 139 atoms and/or larger than 1.46−1.57 nm in diameter), the truncated octahedron is the most stable shape. Within this range, the octahedron is almost as equally stable, although it becomes more stable below 56 atoms/1.12−1.15 nm. The tetrahexahedron is the most stable shape below the 139 atoms/1.46−1.57 nm threshold. The second most stable crystal changes from octahedron to truncated octahedron, then back to octahedron, and finally to tetrahedron for the lowest sizes. The scenarios are depicted in Figure 4.

While the perfect geometrical shapes of nanocrystals can be realized only for specific numbers of atoms, the variational approach applies through a continuum range. The argument becomes critical for small sizes where "magic numbers" of clusters might appear. Therefore, the approach should be considered only for investigating trends in the hierarchy of crystal shapes *versus* sizes. For this purpose, the approach to very small clusters is solely performed to make contact with *ab initio* results. By comparing Figure 1a and 1c, we conclude that our variational approach gives similar shape transitions at slightly smaller sizes than those obtained by *ab initio* calculations. These quantitative differences may be attributed to the considerable surface and core reconstruction of small crystals allowed in *ab initio* calculations (in particular, leading to icosahedral, decahedral *etc.* motifs). In the variational approach, a crystal is considered to have perfect fcc core and facets, and the non-homogeneous near-surface atomic relaxations are included into the model only through the slab calculations of the surface energies. Besides that, the lattice parameter anisotropy, the presence of edges and corners[12] may give an important contribution to the energy of a small crystal. The finite temperature effects may also contribute to these tendencies.[25] Thus, the accuracy of the variational approach increases with size.

Regarding the stability of the tetrahexahedron, our arguments are based exclusively on the variational approach since the *ab initio* calculations of the crystals are beyond current computational capabilities. The minimum (730) slab width achievable without affecting the fcc arrangement is ~0.81 nm. This value is well below the threshold for the tetrahexahedron transition (1.46−1.57 nm) of the crystals, so the model, based on bulk and surface energies of the truncated lattice, is applicable for the (730) case. In addition, the good qualitative agreement of the variational and *ab initio* results for the other six shapes makes us confident about the

qualitative tendency of the tetrahexahedron stability. Furthermore, the experimentally observed Pt tetrahexahedrons (although at larger sizes)[9] corroborate our theoretical conclusions.

Up to now and according to ref 7, cubic crystals have been experimentally observed 15 times, tetrahedron 9 times, truncated octahedron 5 times, cubeoctahedron 3 times, octahedron 2 times, and tetrahexahedron 1 time. To compare experimental data with our results, we should also consider the approximations of the latter. Contributions like crystal shape rounding due to the existence of other facets,[26] phonons, defects,[7] substrate,[26] and modified surface energies due to oxidation or other electrochemical effects are neglected in our theory, whereas they may be essential in experiment. Moreover, the variety of observed Pt crystal shapes demonstrate the possibility to produce metastable shapes by tailoring the preparation conditions. The most frequent observation of cubes and tetrahedrons can be explained by their metastability for small dimensions (Figure 4) that could be potentially preserved during further crystal growth. Such argument is corroborated by the observed decrease of cube frequency during "annealing" and the larger sizes of truncated octahedron in comparison with those of cubes and tetrahedrons.[27] The appearance of truncated octahedron is in agreement with its promoted stability at large sizes as predicted by the variational approach. Conversely, we would expect more frequent observations of octahedrons and tetrahexahedrons, which may require *ad hoc* preparations.[9] The vast majority of nanoparticle syntheses are performed in the presence of surfactants which can affect reactivity and shape the particles. To account for this effect, the model can be extended by adding dependences on further degrees of freedom, such as parametrizing the surface energy dependence on the chemical potential of the adsorbate. Moreover, the stress/strain and chemical effects of edges and corners could be included in a similar fashion.

In conclusion, we have developed a variational approach which combined with *ab initio* calculations allows evaluation of stable and metastable shapes of Pt crystals in a wide range of sizes. Within our approach, the transitions between equilibrium shapes occurring at sizes smaller than ~3 nm are explained by strong dependence of the surface energies with respect to the lattice parameter (surface tension). Within numerical accuracy, the lowest energy Pt crystals change shape from truncated octahedron to tetrahexahedron with decreasing size at around 1.46−1.57 nm diameter. The variety of observed Pt crystal shapes demonstrates the possibility of producing metastable shapes by varying the preparation conditions. Besides, stable (or slightly metastable) shapes at small dimensions might keep their arrangement during grow condition. The combination of the presented variational approach based on *ab initio* calculations with nanofabrication techniques could become fruitful direction for designing new nanosystems with superior chemical, optical, and electronic properties.[1−6,13]

METHODS

***Ab Initio* Calculations.** *Ab initio* calculations are carried out without spin polarization (not required for platinum) at zero temperature and without zero-point motion. The effect of lattice vibrations is omitted. Perfect face center cubic configurations are used as a starting point for relaxations. Numerical convergence to within about 1 meV/atom is ensured by enforcing a high energy cutoff (350 eV). For the bulk EOS, we use dense 24 × 24 × 24 Monkhorst-Pack **k**-point meshes. For the finite crystals, only the Γ-point is considered. For the slabs, the in-plane **k**-point meshes are chosen to be 16 × 16, 16 × 16, and 5 × 1 for (100), (111), and (730), respectively, whereas one **k**-point is used in direction perpendicular to the slabs' direction. For finite crystals and slabs, the shape and volume of the unit cell are fixed to conserve enough vacuum (~12 Å). In addition, the width of the slabs are also fixed to preserve the lattice parameter in all directions. All of the other structural degrees of freedom are relaxed. The surfaces are modeled by using (1 × 1) 2D unit cells. The calculations are performed with our high-throughput framework AFLOW.[28,29] All quantum mechanical energies are obtained from first-principles within the generalized gradient approximation[30] using projector augmented wave pseudopotentials, as implemented in the VASP package.[31] The slab configurations are generated with the online software ACONVASP.[28,29]

To calculate the surface energy, we consider slabs with different width. We use up to 16, 16, and 94 atomic layers for the (100), (111), and (730) cases, respectively. The convergence of the surface energy with respect to the number of layers is evaluated by fitting the slab energies according to the Fiorentini and Methfessel scheme.[32] Thus, the bulk energy is actually never used for the surface calculations.

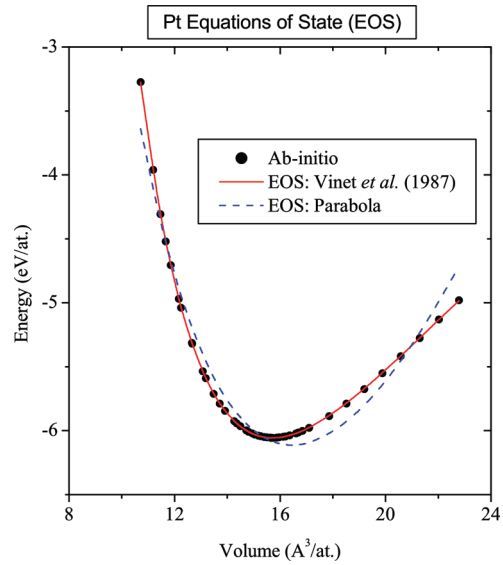

Figure 5. Energy of bulk Pt as a function of volume obtained from first-principles. Dashed and solid lines indicate parabolic and Vinet bulk EOS fits.

TABLE 1. Platinum: Bulk Volume Per Atom (V_0), Lattice Parameter (a_0), Bulk Modulus (B_0), and Bulk Modulus Derivative with Respect to Pressure (B'_0) Obtained from First-Principles and from Experimental Reports

method	V_0 (Å^3)	a_0 (Å)	B_0 (GPa)	B'_0
GGA-PBE (VASP)[a]	15.723	3.977	249	5.55
GGA-PBE (VASP)[b]	16.474	4.039	256	
GGA-PBE (ABINIT)[c]	15.793	3.983	228	6.14
GGA-PBE (FP-LAPW)[d]	15.643	3.97	241	
GGA-PBE (FP-LAPW)[e]	15.761	3.98	259	
LDA (QUANTUM ESPR.)[f]	15.073	3.921	293	5.56
LDA (ABINIT)[c]	14.823	3.899	302	5.61
GGA-PBE (QUANTUM ESPR.)[g]	15.880	3.99	246	
Experiment[h]			278	5.61
Experiment[i]	15.095	3.923		

[a]Present study: Vinet EOS. [b]Present study: parabolic EOS. [c]Vinet EOS (Dewaele *et al.*[34]). [d]Murnaghan EOS (Silva *et al.*[35]). [e]Baud *et al.*[36] [f]Vinet EOS (Menéndez-Proupin *et al.*[33]). [g]Murnaghan EOS (Singh-Miller *et al.*[37]). [h]Holmes *et al.*[38] [i]Villars *et al.*[39]

Bulk Equation of State (Bulk EOS). First-principles data on Pt bulk energy *versus* volume are used to fit two bulk EOS. The parabolic bulk-EOS:

$$E_{\text{bulk}} = E_0 + \frac{1}{2}B_0\frac{(V - V_0)^2}{V_0} \tag{5}$$

and the "Vinet *et al.*" bulk-EOS[24,33]

$$E_{\text{bulk}} = E_0 + \frac{9B_0V_0}{\eta^2}\{1 - e^{\eta(1-X)}[1 - \eta(1 - X)]\}$$
$$\eta = \frac{3}{2}(B'_0 - 1),\ X = \left(\frac{V}{V_0}\right)^{1/3} \tag{6}$$

In eqs 5 and 6, V_0 is the bulk volume per atom, a_0 is lattice parameter, B_0 is bulk modulus, and B'_0 is the bulk modulus derivative with respect to pressure. Note that throughout this section, the *sub-* and *superscript* "0" indicates bulk values.

Ab initio results and the bulk EOS fits are presented in Figure 5. The characteristic values, compared with previously obtained theoretical and experimental data, are also listed in Table 1.

Surface Energy. The volume of cubic (cP), bcc (cI), and fcc (cF) crystal lattices with N sites can be expressed as

$$V = Na^3/L \tag{7}$$

where L is the number of crystal sites per *conventional* cubic unit cell (L = 1, 2, and 4 in the case of cubic, bcc, and fcc lattices) and a is the conventional lattice parameter. The volume of a crystal can be expressed through the edge's length r (the radius in the case of a sphere) as

$$V = r^3K_v \tag{8}$$

where K_v is a *shape coefficient* (Table 2). The combination of eq 7 and eq 8 leads to the expression for the side length r of a regular shape crystal containing N lattices sites with parameter a as

$$r = a\left(\frac{N}{LK_v}\right)^{1/3} \tag{9}$$

The surface area S_{lmn} of (lmn) facets of a regular shape crystal can be written as

$$S_{lmn} = r^2K_s^{lmn} \tag{10}$$

where K_s^{lmn} is a *facet coefficient* (Table 2). From eq 9 and eq 10, we obtain the expression for the surface area of the (lmn) facets of a regular shape crystal with N lattice sites, volume V, and parameter a

$$S_{lmn} = \frac{K_s^{lmn}}{(K_vL)^{2/3}}a^2N^{2/3} = \frac{K_s^{lmn}}{K_v^{2/3}}V^{2/3} \tag{11}$$

In the calculations for the energy for a particle, we variationally minimize the expression eq 1

$$E(a) = E_{\text{bulk}}(a) + \sum_{lmn}\gamma_{lmn}(a)S_{lmn}(a)$$

where $E_{\text{bulk}}(a)$ and $S_{lmn}(a)$ are determined by eqs 6, 7, and 11.

Case of Parabolic Bulk EOS. In the case of parabolic bulk EOS, eq 5 and Figure 5, the energy of a finite crystal becomes

$$E(V) = E_0 + \frac{1}{2}B_0\frac{(V - V_0)^2}{V_0} + \sum_{lmn}\gamma_{lmn}\frac{K_s^{lmn}}{K_v^{2/3}}V^{2/3} \tag{12}$$

The minimization with respect to volume gives

$$\frac{V - V_0}{V_0} = -\frac{2}{3}\frac{1}{V^{1/3}}\frac{\sum_{lmn}K_s^{lmn}\sigma_{lmn}(V)}{B_0K_v^{2/3}} \tag{13}$$

where σ_{lmn} is the surface stress:[40]

$$\sigma_{lmn} = \gamma_{lmn} + \frac{3}{2}V\frac{\partial\gamma_{lmn}}{\partial V} =$$
$$\gamma_{lmn} + a^2\frac{\partial\gamma_{lmn}}{\partial a^2} = \gamma_{lmn} + \frac{a}{2}\frac{\partial\gamma_{lmn}}{\partial a} \tag{14}$$

The nonlinear expression eq 13 defines the crystal volume V as a function of the volume V_0 of the same crystal with the bulk lattice parameter.

In the case of large crystal, eq 13 can be linearized as

$$\left.\frac{V - V_0}{V_0}\right|_{V\to V_0} \simeq -\frac{2}{3}\frac{1}{V_0^{1/3}}\frac{\sum_{lmn}K_s^{lmn}\sigma^0_{lmn}}{B_0K_v^{2/3}} =$$
$$-\frac{2}{3}\frac{1}{r_0}\frac{\sum_{lmn}K_s^{lmn}\sigma^0_{lmn}}{B_0K_v} \tag{15}$$

where σ^0_{lmn} is the bulk surface stress:

$$\sigma^0_{lmn} = \sigma_{lmn}(a_0) \tag{16}$$

If we substitute eq 15 into eq 12 and linearize self-consistently, we obtain

TABLE 2. Values of K_v and K_s^{lmn} Coefficients (eq 8 and eq 10) in the Case of Seven Considered Regular Crystal Shapes Plus the Sphere

	lmn	K_v	K_s^{lmn}
cube	100	1	6
octahedron	111	$\sqrt{2}/3$	$2\sqrt{3}$
tetrahedron	111	$\sqrt{2}/12$	$\sqrt{3}$
cuboctahedron	100	$5\sqrt{2}/3$	6
	111		$2\sqrt{3}$
truncated octahedron	100	$8\sqrt{2}$	6
	111		$12\sqrt{3}$
truncated cube	100	$7(3 + 2\sqrt{2})/3$	$12(1 + \sqrt{2})$
	111		$2\sqrt{3}$
tetrahexahedron	730	10/7	$6\sqrt{1+(3/7)^2}$
sphere		$4\pi/3$	4π

TABLE 3. Values of $2/3(K_s^{lmn}/K_v)$ (eq 15) in the Case of All Considered Regular Shape Crystals Plus the Sphere

	lmn	$2/3(K_s^{lmn})/(K_v)$
cube	100	4
octahedron	111	$4\sqrt{3/2}$
tetrahedron	111	$\sqrt{6}/18$
cuboctahedron	100	$12/(5\sqrt{2})$
	111	$4/5\sqrt{3/2}$
truncated octahedron	100	$(2\sqrt{2})^{-1}$
	111	$\sqrt{3/2}$
truncated cube	100	$24/7(1+\sqrt{2})/(3+2\sqrt{2})$
	111	$4/7(\sqrt{3})/(3+2\sqrt{2})$
tetrahexahedron	730	$14/5\sqrt{1+(3/7)^2}$
sphere		2

$$\left.\frac{E-E_0}{N}\right|_{V\to V_0} \simeq N^{-1/3}a_0^2\frac{\sum_{lmn}K_s^{lmn}\gamma_{lmn}^0}{(K_vL)^{2/3}} \qquad (17)$$

Within this framework, eq 17 shows that the energies (per atom) of large crystals with regular shapes are linear in $N^{-1/3}$ through a geometric coefficient independent of the size of the crystal. Consequently, if eq 15 and eq 17 are considered adequate, then there cannot be any change in the hierarchy of different shapes with respect to size for large crystals. The fact is also demonstrated numerically in Figure 2c for large *N*.

Note that in Figure 1b the case of $\gamma_{lmn} \equiv \gamma_{lmn}^0$ is considered to achieve almost linear dependencies for all the sizes. In this case, eq 13 and eq 15 are transformed by $\sigma_{lmn} \to \gamma_{lmn}^0$, while eq 17 remains invariant.

From the comparison of eq 13 with eq 15, it follows that the bulk surface stress σ_{lmn}^0 is the key factor controlling the lattice parameter of a finite crystal only in the case of large crystals. This happens because the bulk surface stress is determined by the bulk surface energy and its first derivative with respect to the lattice parameter (eq 24). Therefore, any nonlinear dependence of the surface energy on the lattice parameter is not included in the bulk surface stress.

The structural values of $2/3(K_s^{lmn}/K_v)$ are listed in Table 3 for all considered regular shape crystals plus the sphere. For the sphere, cube, and octahedron, the values correspond to those obtained by Stoneham[15] (as an octahedron has eight faces rather than six, there is a misprint in the corresponding expression of ref 15).

Effective Pressure Induced by the Surface of Crystal. The change in the lattice parameter of finite crystal due to the presence of surface can be characterized by an effective "Young−Laplace" pressure *P*.[18,19]

$$P = -\left.\frac{\partial E}{\partial V}\right|_{V=V_0,N=\text{const}} \qquad (18)$$

Substituting eq 1 into eq 18 (with substitutions from eq 6, eq 7, and eq 11), we obtain

TABLE 4. Coefficients of Polynomial Expansion in Equation 22 Obtained by Fitting the Quantum Mechanical Energies (Figure 3a)

i	$\gamma'^{(i)}_{100}$	$\gamma'^{(i)}_{111}$	$\gamma'^{(i)}_{730}$
0	1.83004	1.27741	13.89319
1	−6.79478	−6.01515	−44.03989
2	−115.68222	−102.1737	−858.96575
3	−745.26995	−258.90987	−28840.09589
4	−2655.7435	−4563.9661	
5	2568.98707	11088.1042	
6	−39821.79352	−43067.50223	

TABLE 5. Values for the Bulk Surface Energies γ_{lmn}^0 and Surface Stresses σ_{lmn}^0 for *lmn* = (100), (111), and (730) Calculated in the Present Paper and Compared to Previous Reports[a]

	γ_{lmn}^0 (eV/atom)	γ_{lmn}^0 (J/m²)	γ_{lmn}^0 (meV/Å²)	σ_{lmn}^0 (meV/Å²)
		(100)		
GGA-PBE (VASP) [b]	0.92	1.85	116	331
GGA-PBE (QUANTUM ESPR.) [c]	0.90	1.81	114	
GGA-PW91 (VASP) [d]	0.92	1.84	116	
GGA-PBE (FP-LAPW) [e]	1.16	2.35	147	
		(111)		
GGA-PBE (VASP) [b]	0.64	1.49	93	313
GGA-PBE (QUANTUM ESPR.) [c]	0.65	1.49	95	
GGA-PW91 (VASP) [d]	0.66	1.54	96	
GGA-PBE (FP-LAPW) [e]	0.85	1.99	124	
GGA-PBE (FP-LAPW) [f]	0.71	1.67	104	
GGA-PW91 (PP) [g]	0.66	1.55	97	317
		(730)		
GGA-PBE (VASP) [b]	6.95	1.85	115	298

[a]The surface energies are presented in the three different units used in literature. [b]Present study. [c]Singh-Miller *et al.*[37] [d]Iddir *et al.*[26] [e]Baud *et al.*[36] [f]Silva *et al.*[35] [g]Boisvert *et al.*[41]

$$P = -\frac{2}{3}\left(\frac{L}{N}\right)^{1/3}\frac{1}{a_0}\frac{\sum_{lmn}K_s^{lmn}\sigma_{lmn}^0}{K_v^{2/3}} \qquad (19)$$

or equivalently

$$P = -\frac{2}{3}\frac{1}{V_0^{1/3}}\frac{\sum_{lmn}K_s^{lmn}\sigma_{lmn}^0}{K_v^{2/3}} = -\frac{2}{3}\frac{1}{r_0}\frac{\sum_{lmn}K_s^{lmn}\sigma_{lmn}^0}{K_v} \qquad (20)$$

where the bulk surface stress σ_{lmn}^0 is determined by eq 14 and eq 16. The expressions eq 19 and eq 20 are the generalization of the Laplace−Young equation to the case of crystal with arbitrary shape. By combining eq 15 and eq 20, we obtain a relation between the crystal lattice parameter and the effective surface pressure in the case of large crystals:

$$\left.\frac{V-V_0}{V_0}\right|_{V\to V_0} \simeq \frac{P}{B_0} \qquad (21)$$

Values of γ_{lmn}^0, σ_{lmn}^0 for Pt (100), (111), and (730) Surfaces. The dependencies of the self-consistent surface energy γ'_{lmn} (eq 4) on the lattice parameter can be expanded as

$$\gamma'_{lmn}(a) = \gamma_{lmn}^{(0)} + \gamma_{lmn}^{(1)}X + \gamma_{lmn}^{(2)}X^2 + \ldots \qquad (22)$$

with $X = 1 - a/a_0$. Correspondingly, the bulk surface energies γ_{lmn}^0 and surface stresses σ_{lmn}^0 (eq 14) become

$$\gamma_{lmn}^0 = \frac{\gamma'_{lmn}(a_0)}{2K_{slab}^{lmn}a_0^2} = \frac{\gamma_{lmn}^{(0)}}{2K_{slab}^{lmn}a_0^2} \qquad (23)$$

$$\sigma_{lmn}^0 = \frac{\gamma_{lmn}^{(0)} - 0.5\gamma_{lmn}^{(1)}}{2K_{slab}^{lmn}a_0^2} \qquad (24)$$

By using the coefficients of polynomial expansion eq 22 listed in Table 4, we calculate the bulk surface energies and the surface stresses for the three platinum surfaces. The results compared with other corresponding literature data are reported in

Table 5. The expansion eq 22 can be used as a reference in future studies of Pt surfaces.

Acknowledgment. We acknowledge Wahyu Setyawan, Ohad Levy, and Mike Mehl for fruitful discussions. This research was supported by ONR (N00014-07-1-0878, N00014-07-1-1085, N00014-09-1-0921) and NSF (DMR-0639822). Computational support was provided by TeraGrid resources (TACC, MCA-07S005).

REFERENCES AND NOTES

1. Greeley, J.; Mavrikakis, M. Alloy Catalysts Designed from First Principles. *Nat. Mater.* **2004**, *3*, 810–815.
2. Alayoglu, S.; Nilekar, A. U.; Mavrikakis, M.; Eichhorn, B. Ru−Pt Core−Shell Nanoparticles for Preferential Oxidation of Carbon Monoxide in Hydrogen. *Nat. Mater.* **2008**, *7*, 333–338.
3. Nørskov, J. K.; Bligaard, T.; Rossmeisl, J.; Christensen, C. H. Towards the Computational Design of Solid Catalysts. *Nat. Chem.* **2009**, *1*, 37–46.
4. Nørskov, J. K.; Abild-Pedersen, F. Catalysis: Bond Control in Surface Reactions. *Nature* **2009**, *461*, 1223–1225.
5. Greeley, J.; Stephens, I. E. L.; Bondarenko, A. S.; Johansson, T. P.; Hansen, H. A.; Jaramillo, T. F.; Rossmeisl, J.; Chorkendorff, I.; Nørskov, J. K. Alloys of Platinum and Early Transition Metals as Oxygen Reduction Electrocatalysts. *Nat. Chem.* **2009**, *1*, 552–556.
6. Mayrhofer, K. J. J.; Arenz, M. Fuel Cells: Log on for New Catalysts. *Nat. Chem.* **2009**, *1*, 518–519.
7. Peng, Z.; Yang, H. Designer Platinum Nanoparticles: Control of Shape, Composition in Alloy, Nanostructure and Electrocatalytic Property. *Nano Today* **2009**, *4*, 143–164.
8. Narayanan, R.; El-Sayed, M. A. Shape-dependent Catalytic Activity of Platinum Nanoparticles in Colloidal Solution. *Nano Lett.* **2004**, *4*, 1343–1348.
9. Tian, N.; Zhou, Z.-Y.; Sun, S.-G.; Ding, Y.; Wang, Z. L. Synthesis of Tetrahexahedral Platinum Nanocrystals with High-Index Facets and High Electro-oxidation Activity. *Science* **2007**, *316*, 732–735.
10. Mostafa, S.; Behafarid, F.; Croy, J. R.; Ono, L. K.; Li, L.; Yang, J. C.; Frenkel, A. I.; Cuenya, B. R. Shape-Dependent Catalytic Properties of Pt Nanoparticles. *J. Am. Chem. Soc.* **2010**, *132*, 15714–15719.
11. Cleveland, C. L.; Landman, U. The Energetics and Structure of Nickel Clusters: Size Dependence. *J. Chem. Phys.* **1991**, *94*, 7376–7396.
12. Barnard, A. S.; Zapol, P. A Model for the Phase Stability of Arbitrary Nanoparticles as a Function of Size and Shape. *J. Chem. Phys.* **2004**, *121*, 4276–4283.
13. Burda, C.; Chen, X.; Narayanan, R.; El-Sayed, M. A. Chemistry and Properties of Nanocrystals of Different Shapes. *Chem. Rev.* **2005**, *105*, 1025–1102.
14. Baletto, F.; Ferrando, R. Structural Properties of Nanoclusters: Energetic, Thermodynamic, and Kinetic Effects. *Rev. Mod. Phys.* **2005**, *77*, 371–423.
15. Stoneham, A. M. Measurement of Surface Tension by Lattice Parameter Changes: Theory for Faceted Microcrystals. *J. Phys. C* **1977**, *10*, 1175–1179.
16. Cahn, J. W. Surface Stress and the Chemical Equilibrium of Small Crystals I. The Case of the Isotropic Surface. *Acta Metall. Mater.* **1980**, *28*, 1333–1338.
17. Cahn, J. W.; Lärche, F. Surface Stress and the Chemical Equilibrium of Small Crystals II. Solid Particles Embedded in a Solid Matrix. *Acta Metall. Mater.* **1982**, *30*, 51–56.
18. Harutyunyan, A. R.; Awasthi, N.; Mora, E.; Tokune, T.; Jiang, A.; Setyawan, W.; Bolton, K.; Curtarolo, S. Reduced Carbon Solubility in Fe Nano-clusters and Implications for the Growth of Single-Walled Carbon Nanotubes. *Phys. Rev. Lett.* **2008**, *100*, 195502.
19. Curtarolo, S.; Awasthi, N.; Setyawan, W.; Jiang, A.; Bolton, K.; Harutyunyan, A. R. Influence of Mo on the Fe:Mo:C Nano-catalyst Thermodynamics for Single-Walled Carbon Nanotube Growth. *Phys. Rev. B* **2008**, *78*, 054105.
20. Chepulskii, R. V.; Butler, W.; van de Walle, A.; Curtarolo, S. Surface Segregation in Nanoparticles from First Principles: The Case of FePt. *Scripta Mater.* **2010**, *62*, 179–182.
21. Wasserman, H.; Vermaak, J. On the Determination of the Surface Stress of Copper and Platinum. *Surf. Sci.* **1972**, *32*, 168–174.
22. Solliard, C.; Flueli, M. Surface Stress and Size Effect on the Lattice Parameter in Small Particles of Gold and Platinum. *Surf. Sci.* **1985**, *156*, 487–494.
23. In panels b and c, there is no need for the interpolated reference E^*_{oct}, as the energy can be calculated for any number of atoms. Thus the reference becomes simply E_{oct}.
24. Vinet, P.; Smith, J. R.; Ferrante, J.; Rose, J. H. Temperature Effects on the Universal Equation of State of Solids. *Phys. Rev. B* **1987**, *35*, 1945–1953.
25. Doye, J. P. K.; Calvo, F. Entropic Effects on the Size Dependence of Cluster Structure. *Phys. Rev. Lett.* **2001**, *86*, 3570–3573.
26. Iddir, H.; Komanicky, V.; Öüt, S.; You, H.; Zapol, P. Shape of Platinum Nanoparticles Supported on $SrTiO_3$: Experiment and Theory. *J. Phys. Chem. C* **2007**, *111*, 14782–14789.
27. Petroski, J. M.; Wang, Z. L.; Green, T. C.; El-Sayed, M. A. Kinetically Controlled Growth and Shape Formation Mechanism of Platinum Nanoparticles. *J. Phys. Chem. B* **1998**, *102*, 3316–3320.
28. Curtarolo, S.; Hart, G. L. W.; Setyawan, W.; Mehl, M.; Jahnatek, M.; Chepulskii, R. V.; Levy, O.; Morgan, D. *AFLOW: Software for High-Throughput Calculation of Material Properties*; http://materials.duke.edu/aflow.html, 2010.
29. Setyawan, W.; Curtarolo, S. High-Throughput Electronic Structure Calculations: Challenges and Tools. *Comput. Mater. Sci.* **2010**, *49*, 299–312.
30. Perdew, J. P.; Burke, K.; Ernzerhof, M. Generalized Gradient Approximation Made Simple. *Phys. Rev. Lett.* **1996**, *77*, 3865–3868.
31. Kresse, G.; Hafner, J. *Ab Initio* Molecular Dynamics for Liquid Metals. *Phys. Rev. B* **1993**, *47*, 558–561.
32. Fiorentini, V.; Methfessel, M. Extracting Convergent Surface Energies from Slab Calculations. *J. Phys.: Condens. Matter* **1996**, *8*, 6525–6529.
33. Menéndez-Proupin, E.; Singh, A. K. *Ab Initio* Calculations of Elastic Properties of Compressed Pt. *Phys. Rev. B* **2007**, *76*, 054117.
34. Dewaele, A.; Torrent, M.; Loubeyre, P.; Mezouar, M. Compression Curves of Transition Metals in the Mbar Range: Experiments and Projector Augmented-Wave Calculations. *Phys. Rev. B* **2008**, *78*, 104102.
35. Silva, J. L. D.; Stampfl, C.; Scheffler, M. Converged Properties of Clean Metal Surfaces by All-Electron First-Principles Calculations. *Surf. Sci.* **2006**, *600*, 703–715.
36. Baud, S.; Ramseyer, C.; Bihlmayer, G.; Blügel, S.; Barreteau, C.; Desjonqueres, M. C.; Spanjaard, D.; Bernstein, N. Comparative Study of *Ab Initio* and Tight-Binding Electronic Structure Calculations Applied to Platinum Surfaces. *Phys. Rev. B* **2004**, *70*, 235423.
37. Singh-Miller, N. E.; Marzari, N. Surface Energies, Work Functions, and Surface Relaxations of Low-Index Metallic Surfaces from First Principles. *Phys. Rev. B* **2009**, *80*, 235407.
38. Holmes, N. C.; Moriarty, J. A.; Gathers, G. R.; Nellis, W. J. The Equation of State of Platinum to 660 GPa (6.6 Mbar). *J. Appl. Phys.* **1989**, *66*, 2962–2967.
39. Villars, P.; Calvert, L. *Pearson's Handbook of Crystallographic Data for Intermetallic Phases*, 2nd ed.; ASM International: Materials Park, OH, 1991.
40. Shuttleworth, R. The Surface Tension of Solids. *Proc. Phys. Soc., Sect. A* **1950**, *63*, 444–457.
41. Boisvert, G.; Lewis, L. J.; Scheffler, M. Island Morphology and Adatom Self-Diffusion on Pt(111). *Phys. Rev. B* **1998**, *57*, 1881–1889.